

Initial Results from The Spitzer Young Stellar Cluster Survey

S. T. Megeath¹, L. E. Allen¹, R. A. Gutermuth², J. L. Pipher², P. C. Myers¹, N. Calvet¹, L. Hartmann¹, J. Muzerolle³ & G. G. Fazio¹

ABSTRACT

We report initial results from IRAC observations of four young stellar clusters. These regions are part of a larger *Spitzer* survey of 31 young stellar groups and clusters within 1 kpc of the Sun. In each of the four clusters, there are between 39 and 85 objects with colors inconsistent with reddened stellar photospheres. We identify these objects as young stars with significant emission from circumstellar dust. Applying an analysis developed in a companion paper (Allen et al. 2004), we classify these objects as either pre-main sequence stars with disks (class II) or protostellar objects (class I). These show that the sites of recent star formation are distributed over multi-parsec size scales. In two clusters, Cepheus C and S140, we find protostars embedded in filamentary dark clouds seen against diffuse emission in the IRAC bands.

Subject headings: stars:pre-main sequence — stars: formation — planetary systems:protoplanetary disks — infrared:stars — ISM:clouds — ISM:individual(Cepheus C, S171, S140, NGC 7129)

1. Introduction

In the past 30 years, infrared observations have revolutionized our understanding of star formation. IRAS and ISO observations of young stellar objects showed that young stellar objects with disks and infalling protostellar envelopes exhibit distinctive infrared spectral energy distributions (SEDs) in the mid and far-IR (Wilking & Lada 1983; Adams, Lada, & Shu 1987; Osorio et al. 2003). Ground-based surveys of molecular clouds using near-IR detector arrays found that young stars typically form in clusters (Lada 1992; Carpenter

¹Harvard-Smithsonian Center for Astrophysics, Mail Stop 42, 60 Garden Street, Cambridge, MA 02138 (tmegeath@cfa.harvard.edu)

²Department of Physics and Astronomy, University of Rochester, Rochester, NY 14627

³Steward Observatory, University of Arizona, 933 N. Cherry Ave. Tucson, AZ 85721

2000). The *Spitzer* Space Telescope promises to further revolutionize the study of star formation by providing the capability to image young stellar groups and clusters in the mid-IR with the sensitivity to detect young stars down to the hydrogen burning limit and below. With this new capability, we can build upon the legacies of IRAS, ISO and numerous ground-based near-IR observations by probing the SEDs of stars, brown dwarfs and protostars in young stellar clusters out to distances of 1 kpc or greater.

As part of the Guaranteed Time Observations of the IRAC instrument team, we will image 31 young stellar groups and clusters with the MIPS and IRAC instruments. These have been selected from a catalog of 63 star forming regions within 1 kpc of the Sun containing 10 or more members (Porras et al. 2003). In parallel, we are mapping 7 sq. degrees in the Orion molecular clouds. These surveys will sample the full continuum of multiple star forming regions in the nearest kiloparsec, from small groups of stars in Taurus to the rich Orion Nebula and Mon R2 clusters.

This paper reports on initial results for four young stellar clusters in our sample with properties between those of Taurus and Orion: S140, S171, Cepheus C and NGC7129. These regions are at similar distances, but span a range of FIR luminosities, molecular gas masses, and cluster membership (Table 1). In each cluster, we use the IRAC photometry to identify young stars with disks and protostars. We base our classification on the results of a companion paper by Allen et al. (2004), in which the IRAC colors of the observed young stars are compared to colors derived from models of stars with disks or infalling envelopes.

2. Observations and Data Analysis

Observations of Cepheus C, S171, NGC7129 and S140 were obtained on 2003 December 19, 23, and 24, respectively, with the InfraRed Array Camera (IRAC) (Fazio et al. 2004). Each region was mapped in a 4×3 grid resulting in a $10' \times 15'$ field with coverage in all four IRAC wavelength bands. The 12 second high dynamic range mode was used to obtain two frames at each position, one with an exposure time of 0.4 seconds and one with an exposure time of 10.4 seconds. The map was repeated four times with small offsets, resulting in a total integration of 41.6 seconds per pixel after co-adding the longer duration frames. The observations were processed with the SAO IRAC Pipeline (SIP) and mosaics were created with a custom IDL program.

Source finding and photometry was performed using Gutermuth's Photvis 1.08 which incorporates Landsman's IDLPHOT package into an interactive GUI (Landsman 1993). To subtract out a spatially varying nebulosity, we used an aperture radius of 2 pixels ($2.4''$) and

Table 1: Young Stellar Cluster Properties

Source	Distance ¹ (pc)	IRAS ¹ Luminosity (L _⊙)	Molecular ² Cloud Mass (M _⊙)	Cluster Radius ³ (pc)	Cluster Membership ⁴ (stars)
Cepheus C	700	106	1200	0.3 ⁵	42 ⁵
S171	850	60	870	0.33 ⁶	28 ⁶
S140	900	20560	1290	0.24 ⁷	34 ⁷
NGC 7129	1000	1360	980	0.51 ⁸	80 ⁸

¹Ridge et al. (2003)

²Masses from ¹³CO (1 → 0) data in Ridge et al. (2003)

³Cluster radius derived from an analysis of star counts vs. radius from the cluster center Gutermuth et al. (2004)

⁴Number of detected stars within cluster radius minus the expected number of background stars. The background star density is estimated from a nearby control field

⁵Determined from *K'* mosaic from Hodapp (1994)

⁶Number of sources down to *K* = 15.5

⁷Number of sources down to *K* = 14.5

⁸Number of sources down to *Ks* = 16; Gutermuth et al. (2004)

a sky annulus extending from 2 pixels (2.4") to 6 pixels (7.2"). The calibration of the data was performed with in-flight observations of IRAC standard stars, and aperture corrections were determined for each band from observations of an IRAC standard star. In this paper, we consider only sources detected in all four bands. The standard deviations returned by IDLPHOT includes a contribution of $\sigma(\pi r^2)^{\frac{1}{2}}$, which is added in quadrature, where r is the aperture radius in pixels and σ is the standard deviation of the pixel values in the sky annulus. Consequently, bright, well detected stars can have large uncertainties if they are coincident with a bright, spatially varying nebulosity. Since regions of active star formation often have bright nebulosity in the 5.8 and 8 μm bands, we adopt a maximum photometric uncertainty of 0.25 mag for the 5.8 and 8.0 μm data, as compared to 0.2 mag for the 3.6 and 4.5 μm data. We include only stars brighter than 14 mag at 5.8 μm and 13 mag at 8.0 μm ; at these magnitudes the typical uncertainties are 0.2 mag or less. The resulting median uncertainties are 0.01, 0.01, 0.04 and 0.06 mag, and only 3% of the stars in our sample have uncertainties greater than 0.2 mag in the 5.8 μm and/or 8.0 μm bands. Each image was visually inspected, and nebulous knots misidentified as stars and close double stars were rejected.

3. Classifying young stars using the IRAC color plane

In an analysis of IRAS photometry of young stellar objects in nearby dark clouds, Wilking & Lada (1983) classified young stellar objects as class I, II and III by the slope of their SEDs. The classification scheme was placed in an evolutionary context by Adams, Lada, & Shu (1987), who modeled the SEDs as stars surrounded by dusty disks and envelopes. By comparing these models to the observed SEDs, they identified class I objects as protostars with infalling envelopes and class II objects as stars with disks. Class III objects have the SEDs of stellar photospheres. The three classes are thought to form an evolutionary sequence, with young stars evolving from class I to class II and finally to class III objects (Kenyon & Hartmann 1995).

Instead of performing an analysis directly on the infrared SEDs, we use the colors derived from the four IRAC bands to classify each young star. Figure 1 shows that the [3.6] – [4.5] and [5.8] – [8.0] colors extend over 2 magnitudes. We display two reddening vectors derived from the extinction law of Mathis (1990) and from the optical constants of Draine & Lee (1984). We have applied these two extinction laws to three different sources: a model of Vega (Cohen et al. 1992), a star with disks taken from an ensemble of models by D’Alessio et al. (2004), and an idealized flat spectrum source with $\lambda F_\lambda = \text{constant}$. Since the IRAC 8 μm band overlaps the silicate feature, reddened photospheres would appear increasingly

blue in the $[5.8] - [8.0]$ color; the slope of the reddening vector depends on the extinction law, the intrinsic spectrum of the source, and the amount of extinction.

Centered at $([3.6] - [4.5], [5.8] - [8.0]) = (0, 0)$ are the sources with the colors of stellar photospheres. This region of the color plane may include foreground and background stars as well as diskless (class III) pre-main sequence stars. The distribution of sources appears elongated in the vertical direction; this is due to a combination of reddening and the blue $[3.6] - [4.5]$ colors of background giants with strong CO absorption in the $4.5 \mu\text{m}$ band. In all four clusters there is a concentration of sources centered near $([3.6] - [4.5], [5.8] - [8.0]) = (0.7, 0.5)$, which we outline with a box in Figure 1. These colors can be reproduced by models of disks around young, low-mass stars (Allen et al. 2004; Whitney et al. 2003). The range in colors can be explained largely by variations in inclination and accretion rate (Allen et al. 2004). Based on the range of colors exhibited by the models, we classify objects with $0.0 > ([3.6] - [4.5]) > 0.8$ and $0.4 > ([5.8] - [8.0]) > 1.1$ as class II objects. Although the models also predict stars with $([5.8] - [8.0]) < 0.4$, we have adopted this limit to reliably distinguish class II sources from “colorless” class III/foreground/background stars. Given that only one source in all four regions with $([5.8] - [8.0]) < -0.4$, and assuming that the photometric scatter is symmetric with respect to $([5.8] - [8.0]) = 0$, we estimate the percentage of colorless stars misidentified as Class II sources is less than 1%.

Sources with $([3.6] - [4.5]) > 0.8$ and/or $([5.8] - [8.0]) > 1.1$ cannot be explained by reddened class II objects. These objects have colors similar to those derived from models of protostellar objects with infalling dusty envelopes (Allen et al. 2004; Whitney et al. 2003). We identify these sources as class I objects (we do not distinguish between class 0 and class 1 objects in our current analysis). Several sources in each cluster exhibit colors which are not consistent with models of class I objects, class II objects or reddened photospheres. In Fig. 1, several sources show higher $[3.6] - [4.5]$ colors than class II objects, but lower $[5.8] - [8.0]$ colors than class I or class II objects. Based on the predicted slope of the reddening vector, we identify these nine sources as reddened class II objects. Five sources (three in NGC 7129 and two in S140) have $([5.8] - [8.0]) > 1.1$, consistent with class I objects, but $([3.6] - [4.5]) < 0.4$, which is lower than that predicted by class I models (Allen et al. 2004). Because these sources share the properties of class I and II sources, we refer to these as class I/II sources. These sources are in regions with bright, structured $8 \mu\text{m}$ nebulosity, and these may be class II sources in which compact knots and filaments of nebulosity are contributing to the signal in the $8 \mu\text{m}$ band.

There are several factors that may lead to the incorrect classification of sources. First, models show some overlap between class I sources and class II sources in the IRAC color plane (Allen et al. 2004). We classify the sources in this overlap region as class II. Second,

photometric scatter may alter the classification of a few sources. Third, some of the sources which we have identified as class I objects may be in fact reddened class II objects. Finally, unresolved binaries can result in the incorrect classification of sources. The Herbig Be star LkH α 234 in NGC 7129 is wrongly identified as a class I object in the IRAC color plane; this misclassification is due to a protostellar companion which is detected in ground-based mid-IR observations but is unresolved by IRAC (Cabrit et al. 1999). Background planetary nebulae, AGB stars, and galaxies may also be misidentified as young stars or protostars (Whitney et al. 2003); however, the spatial distribution of sources discussed in the following section indicates that the amount of background contamination is small.

By combining MIPS 24 μ m photometry with the IRAC photometry of NGC 7129, Muzerolle et al. (2004) identify class I and class II objects in NGC 7129 by using the slope of the 1 – 24 μ m SEDs. This data provides an independent check of our classification using the IRAC color plane. For the twenty four sources common to both samples (Muzerolle et al. required detection in *three* IRAC bands *and* the MIPS 24 μ m band), the classification by Muzerolle et al. (2004) is almost entirely consistent with ours (see NGC7129 plot in Fig 1). The one discrepant source has colors consistent with both class II objects and low luminosity class I objects (Allen et al. 2004).

The number of class I and II sources in each cluster is given in Table 2. Our census of class I and class II objects has been demonstrated to be incomplete in NGC7129 by Gutermuth et al. (2004). By requiring detection in only the IRAC 4.5 μ m band and combining the IRAC photometry with ground-based *J* and *H*-band photometry, they find a total of 84 objects with circumstellar disks in NGC7129 within a $9' \times 9'$ field.

Table 2: Statistics on Source Detection and YSO Classification

Source	Total Sources	Class I	Class II	Reddened Class II	Class I/II	Total YSOs
Cepheus C	263	23	55	7	0	85
S171	134	12	27	0	0	39
S140	122	13	22	1	2	38
NGC 7129	119	14	27	1	3	45

4. The Distribution of Young Stars

We show IRAC mosaics of all four clusters in Figures 2 and 3. In preparation for the *Spitzer* young stellar cluster survey, Ridge et al. (2003) mapped each of these regions in the ^{13}CO and C^{18}O ($J = 1 \rightarrow 0$) transition. We overlay contours of the the C^{18}O emission which is an excellent tracer of the structure of the molecular gas in star forming regions (Goldsmith, Bergin & Lis 1997). In comparison, the emission from the more abundant ^{13}CO molecule is stronger and more extended, but has a higher optical depth and is less sensitive to the detailed structure in the gas (Ridge et al. 2003). We find 72% of the class I and 56% of the class II sources fall within the detected C^{18}O emission, and 93% of the class I and 86% of the class II sources fall within the detected ^{13}CO emission. These percentages are qualitatively consistent with the class I sources being younger than the class II sources.

The Cepheus C cluster was first identified in a near-IR survey by Hodapp (1994). In addition to the near-IR cluster, which is located toward the center of Figure 2, the IRAC data show class I and II sources distributed over a 3 pc diameter region. The molecular gas traced by the C^{18}O is visible in the IRAC images as filamentary dark clouds obscuring a diffuse nebulosity extending across the entire mosaic. Two class I objects appear outside the C^{18}O emission; ^{13}CO emission is found toward both of these sources.

The S171 cluster is a compact cluster of young stars found in a bright-rimmed cloud. The OB stars of the Cepheus IV association, which illuminate the bright rim, are outside the image and to the south. The funnel shaped surface of the cloud emits strongly in the IRAC 5.8 and 8.0 μm bands and is clearly seen in Figure 2; the ^{13}CO map shows the molecular gas extending to the edge of the funnel. S171 contains a cluster of young stars near the edge of the cloud; with a dense group of 5 class I sources at northern apex of the cluster. This morphology suggests that star formation is being triggered by a photoevaporation driven shock-wave propagating into the cloud, as first proposed for this region by Sugitani et al. (1995). In addition to the stars in the cluster, there are 6 class II and 2 class I objects spread throughout the molecular cloud. The presence of these stars suggests that a distributed mode of star formation is also occurring in the cloud.

S140 is also a bright-rimmed cloud and the one region of massive star formation in our sample; as in case of S171, the illuminated surface is clearly delineated in Figure 3. A group of at least three early B stars are thought to have recently formed in this region (Evans et al. 1989; Preibisch et al. 2002); these three sources are saturated in our data and appear as a bright extended source near the center of the image. The bright emission from the central stars and the extended nebulosity make the detection of sources in all four bands difficult. We identify three class I and three class II objects within a 0.5 pc radius of the young massive stars; a near-IR star counts analysis reveals 34 members within this radius

(Table 1). Extending east into the molecular clouds is a filamentary dark cloud seen in absorption against the diffuse emission; in these filaments are five class I sources, and three class II sources. Near the eastern edge of the map are two additional class I objects which appear outside the contours of the $C^{18}O$ map; however, ^{13}CO emission is detected toward these sources Ridge et al. (2003). To the southwest of the cluster and outside the bright rimmed cloud are 9 class II objects, a class I object, and a class I/II object. These may be young stars which emerged into the HII region when their natal molecular gas was overtaken by the advancing ionization front.

Near-IR observations show that NGC 7129 contains a cluster of over 80 young stars. Many of these stars are coincident with a bright reflection nebula and cannot be detected in all four IRAC bands; hence the dense clustering of sources found in the near-IR is not apparent in Figure 3. The molecular cloud, as delineated by the $C^{18}O$ contours, wraps around the reflection nebula (Ridge et al. 2003); the distribution of Class I and II sources in Figure 3 shows that star formation is ongoing in this cloud. There are eight class I objects outside the contours of the $C^{18}O$ emission. Emission in ^{13}CO is detected toward all but three of these sources: the northernmost class I object is outside the ^{13}CO map and no molecular gas is detected toward the two class I objects west of the reflection nebula. Gutermuth et al. (2004) and Muzerolle et al. (2004) discuss IRAC and MIPS observations of NGC 7129 in more detail.

5. Discussion

In all four clusters, the young stars and protostars identified by their excess emission in the mid-IR are distributed over multi-parsec distances. In contrast, the diameters of the clusters identified by near-IR star counts are typically 1 pc or less (Lada & Lada 2003). This suggests that a significant fraction of stars in each star forming region form outside the dense clustered regions identified in star counts analyses. Gutermuth et al. (2004) find that half of the stars in NGC 7129 are located in a halo outside the cluster core. Furthermore, star formation in NGC 7129 is continuing in the halo, while the molecular gas has been dispersed toward the cluster core.

The distribution of sources in each region is strikingly different. In Cepheus C, the structure of the molecular cloud breaks up into distinct mid-IR dark cores, and several distinct concentrations of stars are also apparent to the eye. The observed distribution of gas and stars in this region is similar to the hierarchical morphologies generated in numerical models of star formation in turbulent clouds (Bonnell, Bate & Vine 2003). IRAC images of NGC 7129 show a dense cluster of primarily class II sources surrounded by a more extended

halo of class I and II objects. Both S171 and S140 contain compact clusters at the edges of bright-rimmed clouds. These varied morphologies hint that environmental factors, such as the presence of external OB stars, may play a significant role in the formation of clusters.

This work is based on observations made with the *Spitzer* Space Telescope, which is operated by the Jet Propulsion Laboratory, California Institute of Technology under NASA contract 1407. Support for this work was provided by NASA through Contract Number 1256790 issued by JPL/Caltech. Support for the IRAC instrument was provided by NASA through Contract Number 960541 issued by JPL.

REFERENCES

- Adams, F. C., Lada, C. J., & Shu, F. H., 1987, *ApJ*, 312, 788
- Allen, L. E., Calvet, N., D'Alessio, P., Merin, B., Megeath, S. T., Gutermuth, R. A., Pipher, J. L., Hartmann, L., Myers, P. C., & Fazio, G. G., 2004, this volume
- Bonnell, I. A., Bate, M. R., & Vine, S. G. 2003, 343, 413.
- Cabrit, S., Lagage, P.-O., McCaughrean, M., Olofsson, G. 1997, *A&A*, 321, 523
- Carpenter, J. M., 2000, *AJ*, 120, 3139
- Cohen, M., Walker, R. G., Barlow, M. J., & Deacon, J. R. 1992, *AJ*, 104, 1650
- Evans, N. J. II, Mundy, L. G., Kutner, M. L., & DePoy, D. L., 1989, *ApJ*, 346, 212
- Fazio, G. G. 2004, this volume
- D'Alessio, P., Merin, B., Calvet, N. & Hartmann, L. 2004, 2004, in preparation
- Draine, B. T. & Lee, H. M. 1985, *ApJ*, 290, 211
- Goldsmith, P. F., Bergin, E. A. & Lis, D. C., 1997, *ApJ*, 491, 615
- Hodapp, K. W., 1994, *ApJS*, 94, 615
- Kenyon, S. J. & Hartmann, L., 1995, *ApJS*101, 117
- Goodman, A. A., & Arce, H. G., 2004, *ApJ*, in press.
- Gutermuth, R. A., Megeath, S. T., Allen, L. E., Muzerolle, J., Pipher, J. L., Myers, P. C., & Fazio, G. G., 2004, *ApJS*, this volume

- Lada, E. A., 1992, ApJ, 393, 25
- Lada, C. J. & Lada. E. A., 2003, ARA&A, 41, 57
- Landsman, W. B., 1993, Astronomical Data Analysis Software and Systems II, A.S.P. Conference Series, Vol. 52, ed. R. J. Hanisch, R. J. V. Brissenden, and Jeannette Barnes, p. 246
- Mathis, J. S., 1990, ApJ, 28, 37.
- Muzerolle, J., Megeath, S. T., Gutermuth, R. A., Allen, L. E., Pipher, J. L., Gordon, K. D., Morrison, J. E., Rieke, G. H., Myers, P. C., & Fazio, G. G., 2004, ApJS, this volume
- Osorio, M., D’Allesio, P., Muzerolle, J., Calvet, N., & Hartmann, L., 2003, ApJ, 586, 1148
- Preibisch, T. & Smith, M. D. 2002, A&A, 383, 540
- Porras, A., Christopher, M., Allen, L., Di Francesco, J., Megeath, S. T., Myers, P. C., 2003, AJ, 126, 1916
- Sugitani, K., Tamura, M. & Ogura, K. 1995, ApJ, 455, 39
- Ridge, N. A., Wilson, T. L., Megeath, S. T., Allen, L. E., Myers, P. C., 2003, AJ, 126, 286
- Werner, M. 2004, this volume
- Whitney, B. A., Wood, K., Bjorkman, J. E., Cohen, M., 2003, ApJ, 598, 1079
- Wiling, B. A. & Lada, C. J., 1983, ApJ, 274, 693

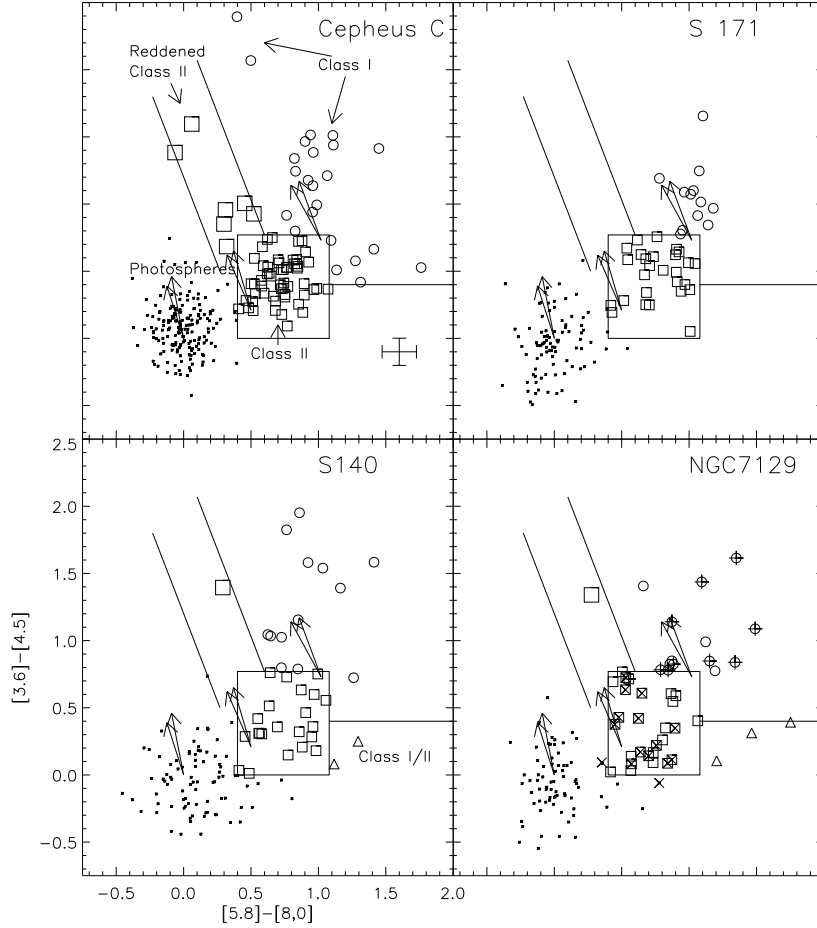


Fig. 1.— The IRAC color-color diagram is displayed for all four clusters. Using a selection criteria outlined in the text and in Allen et al. (2004), the squares are identified as class II sources, the large square are reddened class I sources, and the circles are class I sources. The two parallel lines border the positions of sources we identify as reddened class II objects. In two of the regions, S140 and NGC 7129, we mark the class I/II sources (which share the characteristics of both class I and class II sources) with triangles; the horizontal line above the triangles shows the adopted division between class and class I/II sources. We show reddening vectors for $A_V = 30$ derived from the Draine & Lee (1984) and Mathis (1990) extinction laws, in each case the Draine & Lee (1984) vector points to the left of the Mathis (1990) vector. The vectors were calculated for Vega (at position 0,0), a young star with disks taken from the models of D’Alessio et al. (2004) (0.2,0.5), and a flat spectrum source (0.73,1). Twenty-four sources in NGC7129 were classified using IRAC photometry combined with MIPS 24 μm photometry by Muzerolle et al. (2004); to display these classifications we overplot a plus sign for Class I objects and an X for class II objects. The error bars in the Cepheus C plot show the median uncertainty in the colors for all the sources in all four clusters. A conservative 0.1 mag calibration uncertainty was added in quadrature to the median photometric uncertainty.

Fig. 2.— Images of Cepheus C (top) and S171 (bottom) constructed from the IRAC 3.6 (μm) (blue), 4.5 μm (green) and 8.0 μm (red) images. The contours are the maps of C^{18}O ($1 \rightarrow 0$) emission from Ridge et al. (2003). The C^{18}O observations have an angular resolution of $50''$. We show the position of each young star identified in the IRAC color-color diagram. We mark class II sources with squares, reddened class II objects with large squares, and class I objects with circles. The class I/II sources are marked by triangles.

Fig. 3.— Images of S140 (top) and NGC7129 (bottom) using the the same scheme described in Figure 2

